Electronic Supplementary Information

Destructive Reverse Bias Pinning in Perovskite/Silicon Tandem Solar Modules Caused by Perovskite Hysteresis under Dynamic Shading

Jiadong Qian[a], Marco Ernst*[a], Daniel Walter[a], Md Arafat Mahmud[a], Peter Hacke[b], Klaus Weber[a], Mowafak Al-Jassim[b], and Andrew Blakers[a]

[a.] *Research School of Electrical, Energy and Materials Engineering, The Australian National University, Canberra, ACT, 2600, Australia*
[b.] *National Renewable Energy Laboratory, 15013 Denver W Pkwy, Golden, CO 80401, United States*

Device Fabrication

FTO/glass substrates were successively cleaned with detergent, acetone, isopropanol, ethyl alcohol and deionized (DI) water using an ultrasonic bath. Then the substrates were UV-ozone treated for 15 minutes. Subsequently, ~70 nm of compact TiO_2 (cp-TiO_2) layers and ~80 nm of mesoporous TiO_2 (mp-TiO_2) were deposited on the substrates sequentially. The process description for depositing cp-TiO_2 and mp-TiO_2 layers can be found in Ref [1]. Subsequently, a PMMA:PCBM passivation layer was deposited on the substrate at a spin speed of 4000 rpm for 15 s with an acceleration of 4000 rpm/s. The detailed description for the preparation of PMMA:PCBM passivation solution can be found in Ref [2].

To prepare the quadruple cation perovskite ($Cs_{0.07}Rb_{0.03}FA_{0.765}MA_{0.135}PbI_{2.55}Br_{0.45}$) precursor, 1.1 M formamidinum iodide (FAI), 0.2 M methyl ammonium bromide (MABr), 0.2 M lead bromide ($PbBr_2$), 1.2 M lead iodide (PbI_2), 0.091 M cesium iodide (CsI) and 0.039 M rubidium iodide (RbI) were dissolved in 1 ml mixed solvent of *N,N*-dimethylformamide (DMF) and dimethyl sulfoxide (DMSO) with a volume ratio of 4:1. After covering the substrate with perovskite precursor solution, at first the substrate was rotated at a spin speed of 1000 rpm for 10 s with an acceleration of 100 rpm/s and then at a spin speed of 4000 rpm for 25 s with an acceleration of 1000 rpm/s. During the second step, ~150 µL of chlorobenzene was dripped at the center of the spinning substrate 8 s prior to the end of the spinning program.

Immediately after the spin-coating, the substrates were placed on a hotplate and annealed for 30 minutes at 100 ^{0}C temperature. After cooling down the substrate, 1 mg/ml n-butylammonium iodide (n-BAI) solution in isopropanol was spin-coated on the substrate at a spin speed of 5000 rpm for 15 s with an acceleration of 5000 rpm/s.

The substrates were then annealed on hotplate for 10 minutes at 100 ^{0}C temperature. For hole transport layer (HTL), 2,2′,7,7′-Tetrakis[N,N-di(4-methoxyphenyl)amino]-9,9′-spirobifluorene (Spiro-OMeTAD) solution was prepared by dissolving 73.5 mg Spiro-OMeTAD in 1 ml chlorobenzene and the solution was doped with 17.5 µL of bis(trifluoromethane)sulfonimide lithium salt (Li-TFSI) (520 mg/mL in acetonitrile) and 28.5 µL of 4-tert-butylpyridine. The HTL precursor was spin-coated with spin speed of 3000 rpm for 30 s with an acceleration of 3000 rpm/s. The following day, ~80 nm gold layer was deposited on the coated substrates in thermal evaporation process inside a N_2 filled glovebox. The active area of the cell (0.16 cm^2) was defined using a shadow mask during the evaporation process.

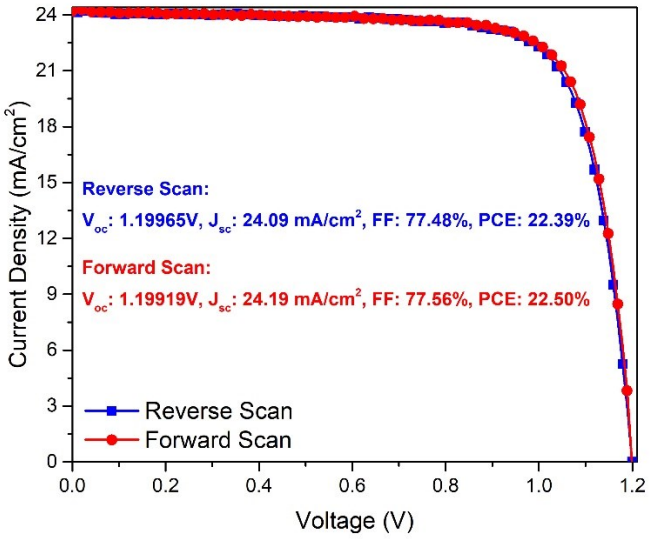

Figure S1 Initial *I-V* characteristics of the sample perovskite cell before the test captured by forward and reverse sweep.

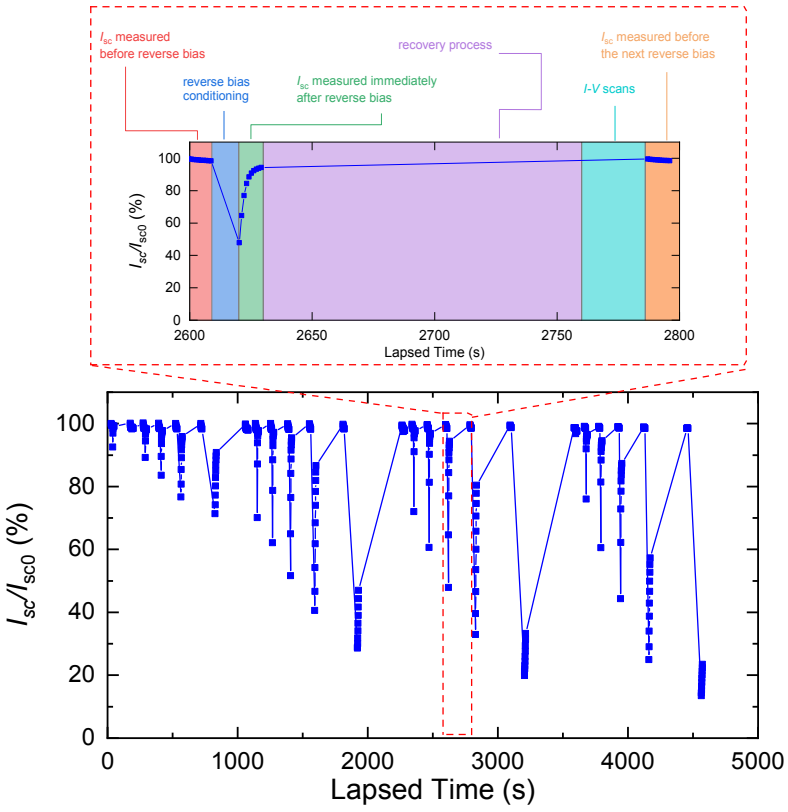

Figure S2 Normalised I_{sc} of the perovskite sample cell during the reverse bias impact effect test. I_{sc} measurements are taken for 10s before the reverse bias conditioning and for another 10s immediately after the reverse bias is applied. Recovery process is considered completed when the cell current at forward bias 1.2 V reaches the level measured at the beginning of the experiment.

Table T1 Cell properties used for reverse bias modelling of PSK/Si tandem modules

	Dimension (cm × cm)	Area (cm^2)	J_{sc} (mA/cm^2)	V_{oc} (V)	Efficiency (%)	*FF* (%)
2T Tandem Module						
perovskite cell	15.6 × 15.6	243.4	19.6	1.05	14.0	68%
silicon cell (filtered)	15.6 × 15.7	244.4	19.5	0.73	11.1	78%
4T Tandem Module						
perovskite cell	2 × 199.5	399	19.6	1.05	14.0	68%

Operating points of a PSK cell after RB

Figure S3 shows that in both case when a 2T tandem module uses either central or module MPPT, the temporary ΔI_{sc} would distort the *I-V* curves of the PSK cell. The module current imposed by the central MPPT is marked with the grey dashed line and equals to 18.1 mA/cm^2. The operating points of PSK cell in a module using module MPPT are selected according to the maximum point current of the module impacted by the distorted PSK *I-V* curve. Whereas in a module MPPT system, the cell operating points plotted in the figure are selected based on the new module maximum power points.

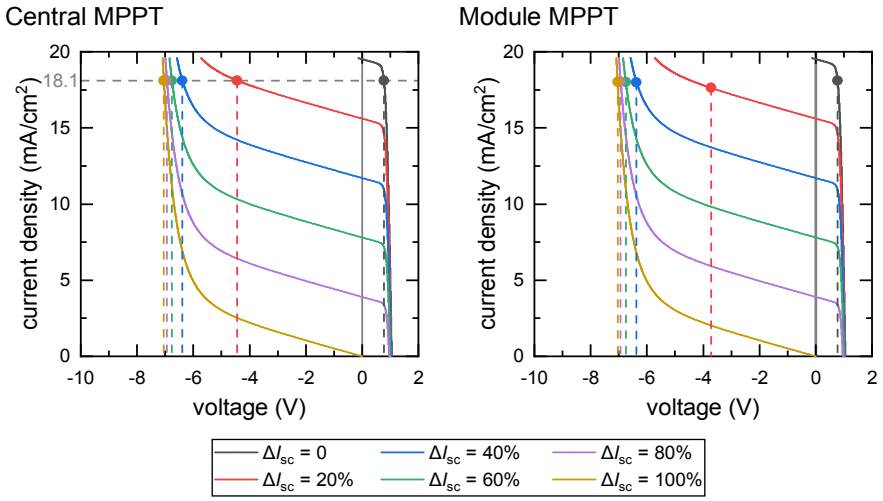

Figure S3 Simulated immediate PSK cell voltage for varied reverse bias induced short-circuit current reduction ΔIsc.

Cell Modelling

The three-layer PSK cell was modelled using numerical device simulations developed at ANU, as described previously [3-5]. Ionic defects are modelled as mobile point charges of fixed number which do not directly act as recombination centres, but which influence recombination rates through electrostatic coupling with electrons and holes in the perovskite layer.

The short circuit-reverse bias-short circuit (SC-RB-SC) protocol was simulated by computing a short dwell period at SC (Figure S4a) followed by a step to RB at a given voltage, and the ion response computed for a specified dwell time (in Figure S4b, -1V for 100s). Subsequently, the cell is returned to SC for 10s, with only the initial SC current reading at 0.2s recorded for the purpose of computing the I_{sc}'/I_{sc} ratio. This roughly corresponds with the time resolution of the measurement used in this work. The integrated recombination current across the perovskite bulk during these voltage cycles were also calculated.

Table T2 lists the parameters used to simulate the results in this work. We note that this is unlikely to be the only parameter space that replicates the experimental data.

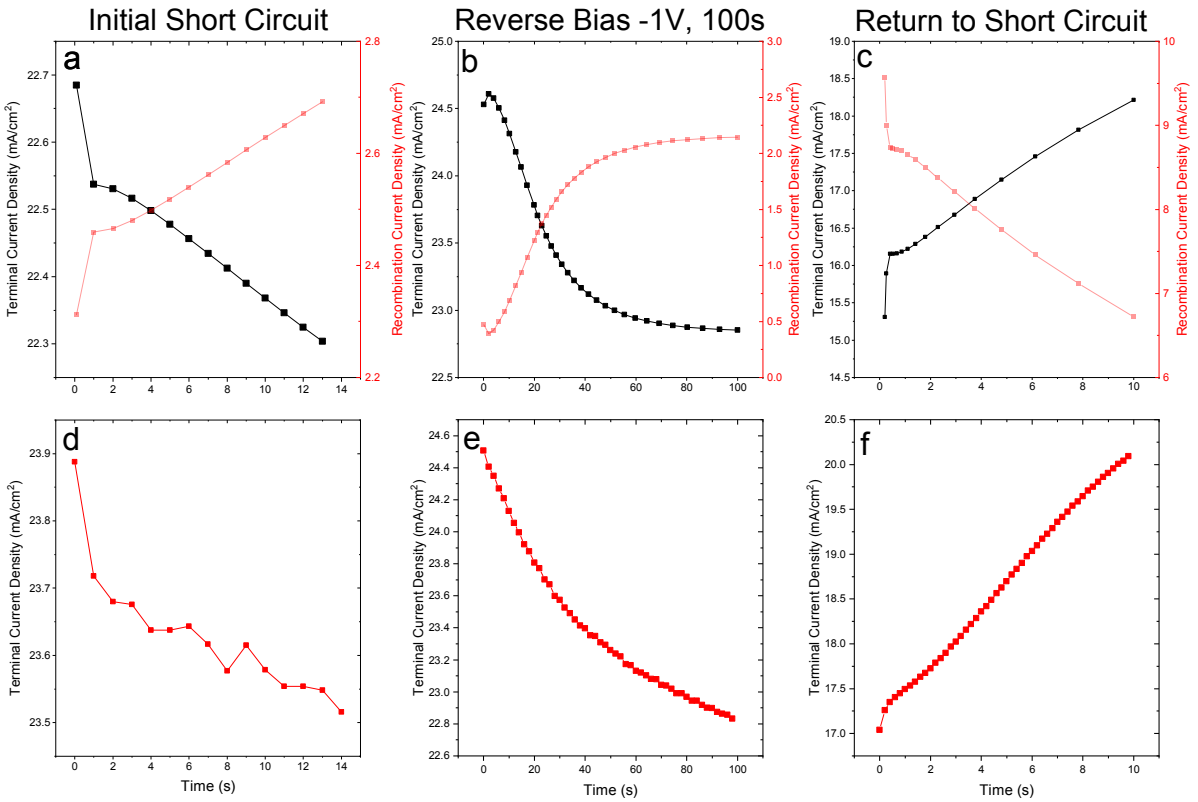

Figure S4 Time series data from short circuit/reverse bias/short circuit protocol taken at -1V, 100s reverse bias dwell (figures d-f). In figures a-c we plot transient simulations using the numerical device model of the equivalent measurement protocol. Also plotted is the time-varying non-radiative recombination current, demonstrating that ion movement alters recombination current losses, which modules the current extracted from the cell terminals.

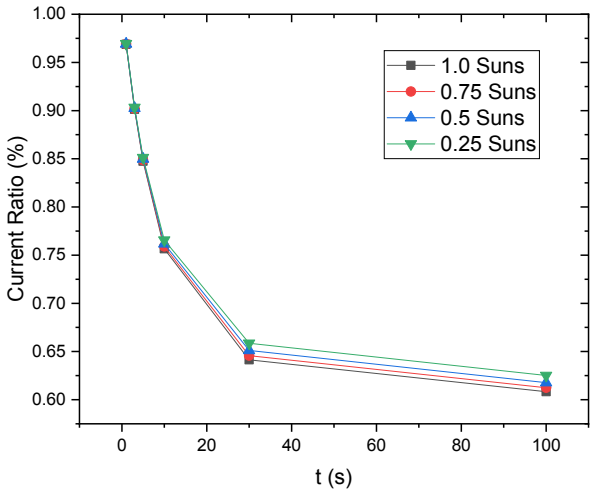

Figure S5 I_{sc}'/I_{sc} ratio computed as a function of illumination level, with an RB voltage of -1.5V. The simulation predicts a dependence on illumination level that is consistent with experiment in direction, but lower in magnitude (Figure 6 of main manuscript). This suggests a light-dependence of ion flux that is not captured by the model.

Table T2 Simulation Parameters

Parameter	Value [unit]	Reference
Hole Transport Layer		
Relative Permittivity	3	
Band Gap	3 [V]	
Electron Affinity	2.2 [V]	
Effective density of states, valence band	10^{20} [cm^{-3}]	
Effective density of states, conduction band	10^{20} [cm^{-3}]	
Electron mobility	0.01 [$cm^2/V{\cdot}s$]	
Hole mobility	0.1 [$cm^2/V{\cdot}s$]	
Dopant defect concentration (p-type)	10^{18} [cm^{-3}]	
Thickness	170 [nm]	
Electron Transport Layer		
Relative Permittivity	24	[6]
Band Gap	3 [V]	
Electron Affinity	3.9 [V]	
Effective density of states, valence band	10^{20} [cm^{-3}]	
Effective density of states, conduction band	10^{20} [cm^{-3}]	
Electron mobility	2 [$cm^2/V{\cdot}s$]	
Hole mobility	0.01 [$cm^2/V{\cdot}s$]	
Dopant defect concentration (n-type)	10^{17} [cm^{-3}]	
Thickness	150 [nm]	

Table T2 (continued) Simulation Parameters

Parameter	Value [unit]	Reference
Perovskite Layer		
Relative Permittivity	64	[7]
Band Gap	1.65 [V]	[8]
Electron affinity	3.9 [V]	
Effective density of states, valence band	10^{19} [cm^{-3}]	
Effective density of states, conduction band	10^{19} [cm^{-3}]	
Electron mobility	2 [$cm^2/V{\cdot}s$]	
Hole mobility	2 [$cm^2/V{\cdot}s$]	
Direct recombination coefficient	7×10^{-10} [cm^3/s]	[9]
Photocurrent density, when illuminated	25 [mA/cm^2]	
Thickness	400 [nm]	
SRH Lifetime, holes	30 [ns]	
SRH Lifetime, electrons	30 [ns]	
Ion Properties		
Positive ion defect concentration	6×10^{17} [cm^{-3}]	
Negative ion defect concentration	1×10^{17} [cm^{-3}]	
Positive ion defect diffusivity	4×10^{-12} [cm^2/s]	
Negative ion defect diffusivity	5×10^{-10} [cm^2/s]	

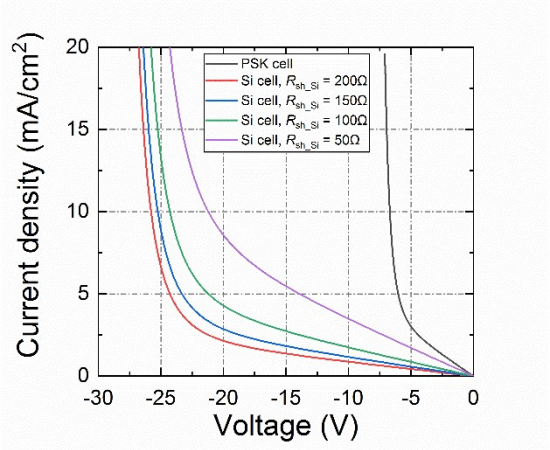

Figure S6 Reverse bias *I-V* characteristics of four Si cells with R_{sh} = 50 Ω, 100 Ω, 150 Ω and 200 Ω, in comparison with the reverse bias characteristics of the sample perovskite cell.

References

[1] J. Peng, J. I. Khan, W. Liu, E. Ugur, T. Duong, Y. Wu, H. Shen, K. Wang, H. Dang, E. Aydin, X. Yang, Y. Wan, K. J. Weber, K. R. Catchpole, F. Laquai, S. De Wolf and T. P. White, *Adv. Energy Mater.*, 2018, **8**, 1801208.

[2] J. Peng, Y. Wu, W. Ye, D. A. Jacobs, H. Shen, X. Fu, Y. Wan, T. Duong, N. Wu, C. Barugkin, H. T. Nguyen, D. Zhong, J. Li, T. Lu, Y. Liu, M. N. Lockrey, K. J. Weber, K. R. Catchpole and T. P. White, *Energy Environ. Sci.,* 2017,**10**, 1792-1800.

[3] D. A. Jacobs, Y. Wu, H. Shen, C. Barugkin, F. J. Beck, T. P. White, K. Weber and K. R. Catchpole, *Physical chemistry chemical physics: PCCP*, 2017, **19**, 3094–3103.

[4] D. Walter, A. Fell, Y. Wu, T. Duong, C. Barugkin, N. Wu, T. White and K. Weber, *J. Phys. Chem. C*, 2018, **122**, 11270–11281.

[5] D. A. Jacobs, H. Shen, F. Pfeffer, J. Peng, T. P. White, F. J. Beck and K. R. Catchpole, *Journal of Applied Physics*, 2018, **124**, 225702.

[6] M. D. Stamate, *Applied Surface Science*, 2003, **218**, 318–323.

[7] I. Anusca, S. Balčiūnas, P. Gemeiner, Š. Svirskas, M. Sanlialp, G. Lackner, C. Fettkenhauer, J. Belovickis, V. Samulionis, M. Ivanov, B. Dkhil, J. Banys, V. V. Shvartsman and D. C. Lupascu, *Advanced Energy Materials*, 2017, **7**, 1700600.

[8] M. M. Lee, J. Teuscher, T. Miyasaka, T. N. Murakami and H. J. Snaith, *Science*, 2012, **338**, 643–647.

[9] T. W. Crothers, R. L. Milot, J. B. Patel, E. S. Parrott, J. Schlipf, P. Müller-Buschbaum, M. B. Johnston and L. M. Herz, *Nano Lett*, 2017, **17**, 5782–5789.